remote sensing

MDPI

Article

Preliminary Inter-Comparison between AHI, VIIRS and MODIS Clear-Sky Ocean Radiances for Accurate SST Retrievals

Xingming Liang [1,2,*], Alexander Ignatov [1], Maxim Kramar [1,3] and Fangfang Yu [1,4]

1 NOAA Center for Satellite Application and Research (STAR), College Park, MD 20740, USA; Alex.Ignatov@noaa.gov (A.I.); Maxim.Kramar@noaa.gov (M.K.); Fangfang.Yu@noaa.gov (F.Y.)
2 CSU, Cooperative Institute for Research in the Atmospheres (CIRA), Fort Collins, CO 80523, USA
3 GST Inc., Greenbelt, MD 20740, USA
4 ERT Inc., Laurel, MD 20707, USA
* Correspondence: Xingming.Liang@noaa.gov; Tel.: +1-301-683-3362; Fax: +1-301-683-3301

Academic Editors: Changyong Cao, Magaly Koch and Prasad S. Thenkabail
Received: 19 November 2015; Accepted: 18 February 2016; Published: 1 March 2016

Abstract: Clear-sky brightness temperatures (BT) in five bands of the Advanced Himawari Imager (AHI; flown onboard Himawari-8 satellite) centered at 3.9, 8.6, 10.4, 11.2, and 12.3 μm (denoted by IR37, IR86, IR10, IR11, and IR12, respectively) are used in the NOAA Advanced Clear-Sky Processor for Oceans (ACSPO) sea surface temperature (SST) retrieval system. Here, AHI BTs are preliminarily evaluated for stability and consistency with the corresponding VIIRS and MODIS BTs, using the sensor observation minus model simulation (O-M) biases and corresponding double differences. The objective is to ensure accurate and consistent SST products from the polar and geo sensors, and to prepare for the launch of the GOES-R satellite in 2016. All five AHI SST bands are found to be largely in-family with their polar counterparts, but biased low relative to the VIIRS and MODIS (which, in turn, were found to be stable and consistent, except for Terra IR86, which is biased high by 1.5 K). The negative biases are larger in IR37 and IR12 (up to ~−0.5 K), followed by the three remaining longwave IR bands IR86, IR10, and IR11 (from −0.3 to −0.4 K). These negative biases may be in part due to the uncertainties in AHI calibration and characterization, although uncertainties in the coefficients of the Community Radiative Transfer Model (CRTM, used to generate the "M" term) may also contribute. Work is underway to add AHI analyses in the NOAA Monitoring of IR Clear-Sky Radiances over Oceans for SST (MICROS) system and improve AHI BTs by collaborating with the sensor calibration and CRTM teams. The Advanced Baseline Imager (ABI) analyses will be also added in MICROS when GOES-R is launched in late 2016 and the ABI IR data become available.

Keywords: SST; AHI; VIIRS; MODIS; Himawari-8; S-NPP; Terra; Aqua; MICROS; ACSPO

1. Introduction

With the launch of the first Visible Infrared Imager Radiometer Suite (VIIRS) onboard the Suomi National Polar Partnership (S-NPP) satellite in October 2011, NOAA has entered a new era of the polar-orbiting environmental satellite operations. Four more VIIRS sensors will fly onboard the follow-on US Joint Polar Satellite System (JPSS) satellites, J1–J4, planned for launch from 2017 to 2026. With its improved spatial and spectral resolution, and radiometric accuracy and stability, the VIIRS instrument is in many ways superior to its operational and research predecessors, the Advanced Very High Resolution Radiometers (AVHRR) flown onboard multiple NOAA and Meteorological Operational (Metop) satellites, and the NASA Moderate-resolution Imaging Spectroradiometers (MODIS) flown onboard Terra and Aqua satellites [1–3].

The NOAA geostationary satellite fleet is also due for a major upgrade, with the launch of the first Advanced Baseline Imager (ABI) onboard the Geostationary Operational Environmental Satellite-R (GOES-R) in October 2016 [4]. The Himawari-8 (H8) geostationary satellite, launched by the Japan Aerospace Exploration Agency (JAXA) in October 2014 and declared operational by the Japan Meteorological Agency (JMA) in July 2015, carries the Advanced Himawari Imager (AHI) onboard, a very close proxy of the ABI. The ABI/AHI sensors have significantly improved upon their predecessors, the imagers onboard the US GOES and Japanese Multi-functional Transport Satellites (MTSAT) [5,6]. In July 2015, the JMA switched over the satellite operations from MTSAT-2 (also known as Himawari-7) to H8, and designated the MTSAT-2 as a standby satellite [7].

Both VIIRS and ABI/AHI provide enhanced capabilities for weather and climate monitoring. Sea surface temperature (SST) is one of the key environmental variables, derived from the clear-sky brightness temperatures (BTs) over ocean in the window bands. Assessing the radiometric accuracy, stability, and cross-platform consistency of the VIIRS and ABI/AHI BTs is critically important to ensure accurate, stable, and consistent SST records from the current polar and geostationary sensors. In this study, we preliminarily cross-evaluate the AHI and VIIRS BTs, in support of the H8 and S-NPP SST production at NOAA, and in preparation for the future GOES-R and JPSS SST operations.

VIIRS and AHI SST retrievals are performed at NOAA using the Advanced Clear Sky Processor for Ocean (ACSPO) system. In addition to the primary SST product, ACSPO also reports the top-of-atmosphere (TOA) BTs over the ocean in the window bands [8]. The clear-sky ocean pixels are identified using the ACSPO clear-sky mask [9]. The clear-sky sensor BTs are another NOAA product, which can be directly assimilated in the Numerical Weather Prediction (NWP) models. To facilitate their validation, the simulated BTs are also calculated in ACSPO using the Community Radiative Transfer Model (CRTM) [10], with the National Centers for Environmental Prediction Global Forecast System (NCEP GFS) [11] upper air fields and the Canadian Meteorological Centre daily L4 SST analysis (CMC 0.2°) [12] as inputs. The model BTs can be used to validate the sensor BTs, among many other applications [13,14].

ACSPO system is operational at NOAA with the S-NPP VIIRS and with several Advanced Very High Resolution Radiometers (AVHRR) Global Area Coverage (GAC; 4 km resolution) onboard NOAA satellites, and with AVHRR Full Resolution Area Coverage (FRAC; 1 km) onboard Metop satellites. Data of two MODIS, onboard Terra and Aqua, and AHI, onboard H8, are also routinely processed in an experimental mode. The SST and model minus observation (M-O, which in this study are inverted to O-M, to facilitate analyses of sensor BTs) biases are monitored in near real-time (NRT) using the Monitoring of IR Clear-Sky Radiances over Oceans for SST (MICROS) web-based system [13,15]. The previous evaluation of the AVHRR, MODIS, and VIIRS radiometric stability and cross-platform consistency in the three SST bands historically used in ACSPO (IR37, IR11, and IR12) confirmed that the VIIRS is a stable and well-calibrated sensor [14]. MODIS BTs were also found to be generally consistent with VIIRS BTs (with the exception of the IR37 on Aqua, which was ~0.2 K out of the VIIRS and Terra family).

With the launch of H8, the ACSPO system was adapted to process AHI data. Note that AHI has five IR window bands, centered at 3.9 (band 7), 8.6 (11), 10.4 (13), 11.2 (14), and 12.4 μm (15). Some of these bands are unique to the AHI/ABI (e.g., *cf.* the three-band configuration in the longwave atmospheric window, IR10/IR11/IR12, with the customary IR11/IR12 two-band configuration on the polar sensors). Additionally, AHI and ABI have an IR86 band. A similar band is also available on MODIS and VIIRS, but not on AVHRR, and so far has not been explored in the ACSPO processing. These new bands are instrumental for SST and clear-sky mask (in particular, to ensure their day/night continuity) and they are currently being actively explored in ACSPO. The MICROS system is also being updated to include the AHI data and to prepare for monitoring of the GOES-R ABI, and to include the new SST bands.

This paper documents preliminary analyses of the AHI O-M biases in all five SST bands, with the emphasis on comparisons with the corresponding VIIRS and MODIS O-M biases. The double

differences are also analyzed to evaluate the SST radiances from the three sensors for stability and cross-platform consistency, and to get ready for the GOES-R ABI planned for launch in 2016.

2. SST Bands and ACSPO Data Selection

2.1. AHI, VIIRS, and MODIS SST Bands

Sensor bands analyzed in this study are summarized in Table 1, and the corresponding relative sensor response functions (SRFs) are shown in Figure 1.

Table 1. AHI, VIIRS, and MODIS SST bands (B: band; CW: center wavelength; SR: spectral range).

Band Name	AHI			VIIRS			MODIS		
	B	CW (μm)	SR (μm)	B	CW (μm)	SR (μm)	B	CW (μm)	SR (μm)
IR37	7	3.85	3.59–4.11	M12	3.70	3.66–3.84	20	3.75	3.66–3.84
IR86	11	8.60	8.12–9.07	M14	8.58	8.40–8.70	29	8.55	8.40–8.70
IR10	13	10.45	9.90–10.96						
IR11	14	11.20	10.31–12.18	M15	10.73	10.26–11.26	31	11.03	10.78–11.28
IR12	15	12.35	11.17–13.66	M16	11.85	11.54–12.49	32	12.02	11.77–12.27

The MODIS and VIIRS SRFs were provided by the NASA MODIS calibration support team (MCST) and by the VIIRS calibration team at the University of Wisconsin, respectively. The AHI SRFs were obtained from the JMA AHI imager website [7]. Here, the bands centered at 3.7/3.9, 8.6, 10.5, 10.7/11.0/11.2, and 11.9/12.0/12.4 μm are denoted IR37, IR86, IR10, IR11, and IR12, respectively, consistently for all three sensors. Note, however, that their SRFs, center wavelengths, and bandwidths do differ. In the atmospheric windows away from the absorption lines, these spectral variations are expected to only minimally affect the TOA BTs. Recall that the previous comparisons between different AVHRR, MODIS, and VIIRS sensors in [14] have shown that the corresponding O-M biases are typically within several hundredths of a Kelvin in the three bands—IR37, IR11, and IR12. The AHI IR37 SRF is shifted to the smaller wavenumbers (longer wavelengths) and covers two N_2O absorption lines around 3.9 μm [16]. Similar SRF behavior is found in the spectrally wide AVHRR band IR37, which however results in only minimal differences between the AVHRR, MODIS, and VIIRS [14]. Note that in addition to the band 20 centered at 3.7 μm, MODIS also has band 22 centered at 3.9 μm and band 23 centered at 4.0 μm, which can be used in concert with band 20 for more accurate nighttime SST retrievals [17]. However, similar bands are not available on VIIRS and AHI, and are beyond the scope of this study, which is focused on the comparison between these three sensors.

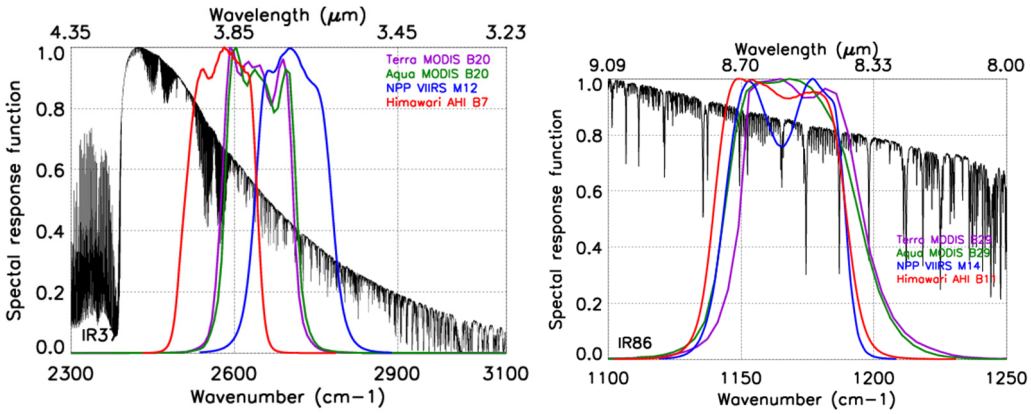

Figure 1. *Cont.*

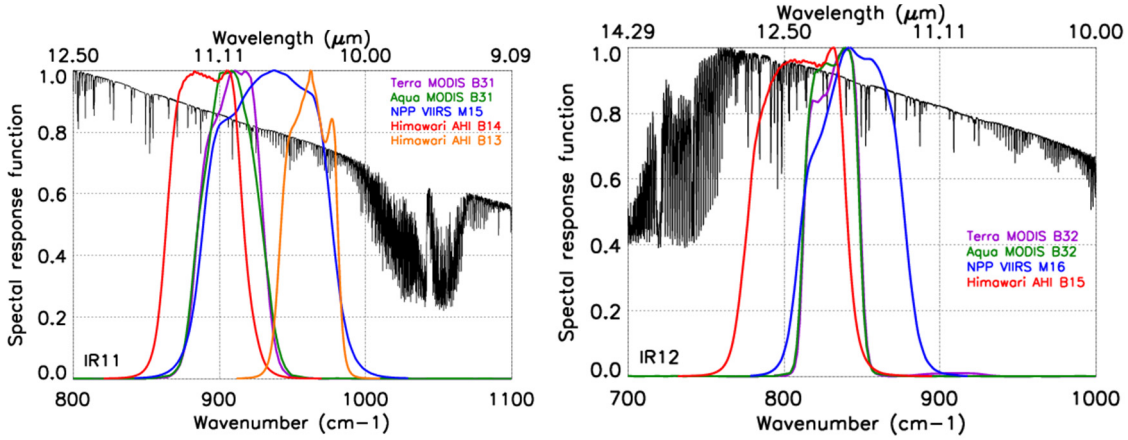

Figure 1. Relative Sensor spectral response functions for IR37 (MODIS B20, VIIRS M12, AHI B7), IR86 (MODIS B29, VIIRS M14 and AHI B11), IR11 (MODIS B31, VIIRS M15, AHI B13 and B14), and IR12 (MODIS B32, VIIRS M16, AHI B15). The scaled TOA radiances (black, scaled at maximum) are superimposed, calculated with Line-By-Line Radiative Transfer Model (LBLRTM, http://rtweb.aer.com/lblrtm_frame.html) using an average atmospheric profile over the 81 ECMWF profiles commonly used for training CRTM coefficients.

2.2. Data

The VIIRS and MODIS provide near-global coverage twice daily, during both day and night, in a swath of ~3040 km (2330 km for MODIS), at 0.75 km resolution at nadir and ~1.5 km at swath edge (1 and 5 km for MODIS, respectively). The ACSPO clear-sky mask identifies from 100–130 M (38–45 M for MODIS) clear-sky pixels on both day and night sides of the Earth ("M" stands for million.)

The H8 is positioned over the equator at 140.7°E. The AHI generates global full disk (FD) images every 10 min, resulting in a total of 142 FD images per day (two slots at 02:40 and 14:40 UTC are reserved for the housekeeping operations). With 2 km resolution at nadir (which degrades to ~6.5 km at view zenith angle, VZA ~ 70°), each AHI FD image comprises a total of 5500 × 5500 pixels, of which from 2.5–5.0 M are identified as clear SST pixels by the current ACSPO clear-sky mask.

Cross-sensor comparisons in MICROS employ double differences (DD) defined as follows [11,12]:

$$\text{SAT} - \text{H8} \;=\; mean\,(\text{SAT}\,[\text{O-M}]) - mean\,(\text{H8}\,[\text{O-M}]) \tag{1}$$

Here, the H8 is used as a reference, and SAT may denote the S-NPP, Terra, or Aqua, which are all evaluated against the H8. To approximately represent the AHI domain, VIIRS and MODIS data were sub-sampled within ±90° longitude around the ~140.7°E H8 sub-satellite point (the latitude range in the sub-sampling was retained from −90° to +90°). The mean is calculated over the full domain for H8, and over the corresponding subsamples for the polar satellite data. Additionally, the VZA for AHI was restricted to <70°, consistently with the maximum VZAs for VIIRS and MODIS. Note that the "M" terms can be accurately calculated for large VZAs with the CRTM which takes into account the sphericity of the Earth [13,14].

2.3. Observation Time and Matchup

Polar sun-synchronous satellites observe the same target on Earth twice daily, during the day and at night, at approximately same local times (LT). Recall that for the afternoon ("PM") S-NPP and Aqua, the Equatorial Crossing Time (ECT) is ~1:30 pm/am LT whereas for the mid-morning ("AM") Terra, the ECT is ~10:30 am/pm LT. The actual LT "in-pixel" is approximately centered at these ECTs but may vary within several hours, depending on the latitude (due to orbital inclination) and pixel position in the scan. Between the AM and PM platforms, the LT differs by 3:00 h on average. At night, the effect

of the diurnal cycle is minimal, and the corresponding global mean O-M biases differ by no more than several hundredths of a Kelvin [14]. During the daytime, diurnal variability, and the corresponding sensitivity of the O-M biases to LT differences, is larger. In MICROS, all polar analyses are stratified by day and night, and using nighttime data (*i.e.*, data with the solar zenith angle, SZA > 90°) is preferred for cross-platform comparisons [8,13,14].

The 10-min AHI FDs provide continuous coverage of the full diurnal cycle, with each FD image covering a wide range of different time zones, often including day and night. Special provision should be made when polar and geo data are compared. In this study, the LT was calculated for each VIIRS, MODIS, and AHI pixel, given its Coordinated Universal Time (UTC) and longitude, and stratified into hourly LT bins. Figure 2 shows the number of clear-sky ocean pixels (NCSOP) in each LT bin, for one full day of 2 June 2015. For AHI, the LT distribution is nearly uniform with ~18 M pixels per hour, whereas the VIIRS and MODIS data are clustered in 3–4 daytime, and 3–4 nighttime bins, centered approximately at the satellite ECTs (~1:30 a.m./p.m. for VIIRS and Aqua, and ~10:30 am/pm for Terra). The NCSOP in the most populated (central) polar bins are ~15 M, ~12 M, and ~27 M for Terra, Aqua, and S-NPP, respectively, and these numbers are reduced ~3~5 times in the adjacent neighboring bins. The sparsely populated polar bins (with NCSOP < 1% of the total sample) were removed, to minimize the outliers.

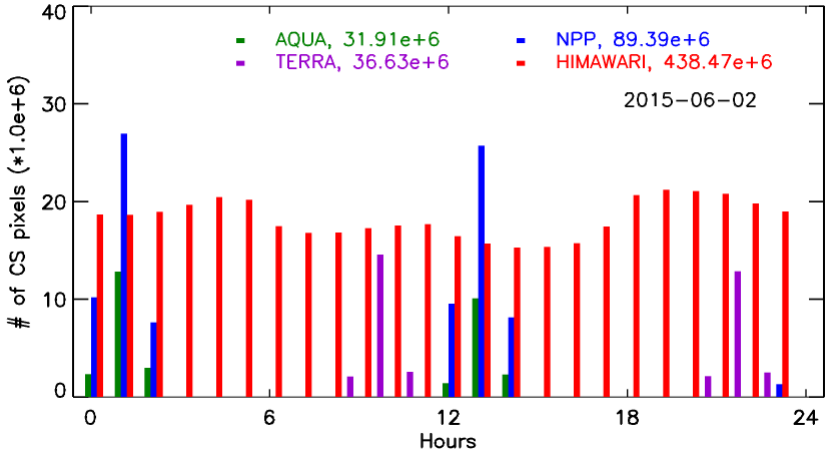

Figure 2. The number of clear-sky pixels in every hour of local time for the day of 2 June 2015 (polar data are sub-sampled to represent the H8 domain).

In what follows, only nighttime data are used to eliminate and minimize the effect of the diurnal cycle and solar refection. The exception is only made when the diurnal cycle is analyzed. In all cases, the specifics of the data sample used in each particular case are explicitly defined.

3. Results and Discussion

3.1. O-M Biases on 2 June 2015

Evaluation of the AHI O-M biases by the NOAA SST team commenced in February 2015, when the first AHI IR data were made available to NOAA by the JMA. The results have been continuously reported to the NOAA AHI/ABI calibration team and used to improve the sensor calibration. While the H8 was declared operational by the JMA in early July 2015, this study uses one month of AHI data from 28 May–27 June 2015. Though still in a commissioning phase, the NOAA AHI/ABI calibration team has confirmed that the calibration in the five IR window bands has not changed.

Figure 3 shows geographical distribution of the nighttime O-M biases in IR37 from S-NPP VIIRS and H8 AHI on 2 June 2015. Note that the H8 has no data around the FD Earth limb, due to the VZA < 70° cut off. The cloud patterns and coverage are similar between the polar and geo sensors. However, the AHI BTs are biased negative relative to the VIIRS.

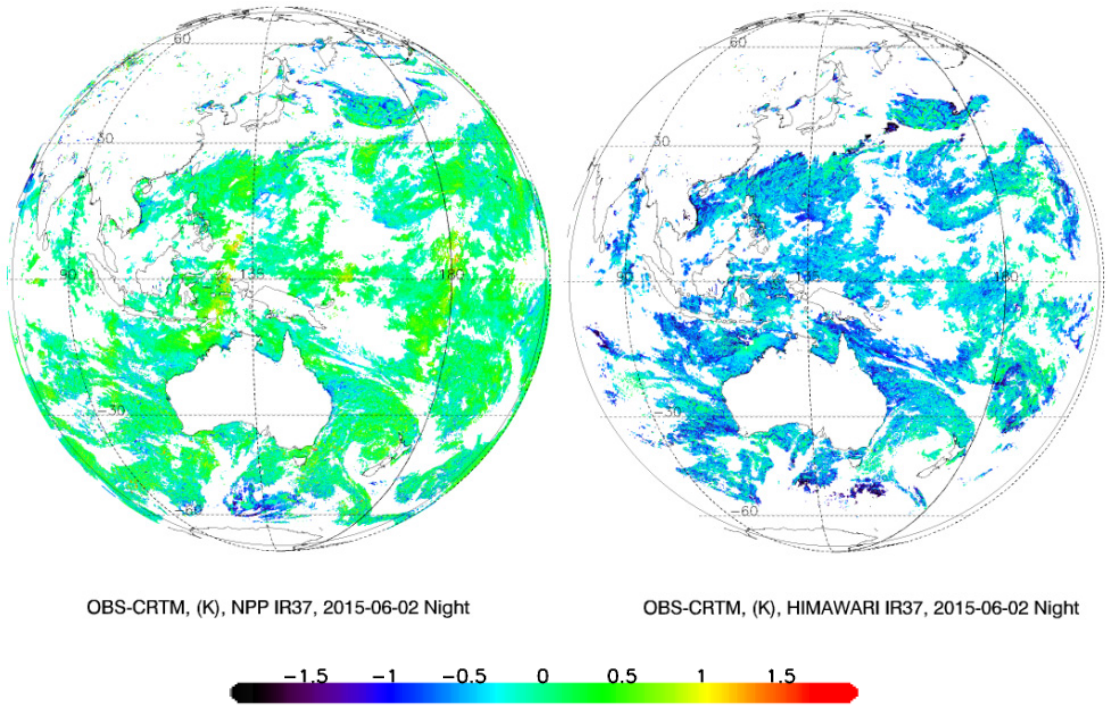

Figure 3. Nighttime O-M biases in IR37 for S-NPP VIIRS and H8 AHI. Data are gridded to 1° × 1°. For VIIRS, nighttime data are defined as those with solar zenith angle, SZA > 90°. For AHI, only data from 1–2 a.m. LT were used (which come from different FD images taken at different UTC times). If more than one VIIRS overpass or AHI FD image satisfying these conditions were available, they were all averaged within a 1° box, for mapping purposes.

Figure 4 shows global histograms of the O-M biases in the domain of Figure 3, but in the IR86 band. The shape is close to Gaussian, for all sensors. Terra shows a large anomaly, due to the electronic cross-talk in IR86 [18]. Other than this known and documented problem, the Aqua and H8 bracket the S-NPP within ~±0.25 K, with the AHI found on the cold end of the family. Note that the IR86 band was not analyzed before [14] and work is currently underway to add it in MICROS.

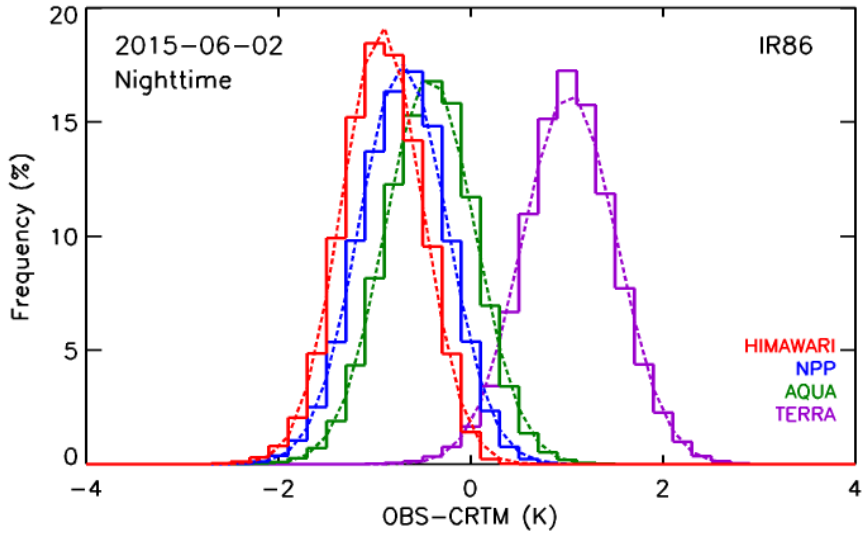

Figure 4. Histograms of the nighttime O-M biases in IR86. Corresponding statistics are listed in Table 2. The dotted lines are Gaussian fits corresponding to the median and robust standard deviation.

Table 2 shows the first and second order O-M statistics for IR86 from Figure 4, as well as for the other four SST bands. In all cases, AHI is in family, although on its low end. In the IR37, the AHI bias with respect to VIIRS is ~−0.5 K. A smaller negative bias of ~−0.3 K is seen in Aqua IR37. This bias was previously observed and attributed to the suboptimal characterization of the Aqua IR37 [14]. The S-NPP and Terra agree to within 0.06 K. In the IR11 and IR12, all three polar sensors closely agree to within several hundredths of a Kelvin, whereas AHI is again biased cold, from ~−0.3 to –0.5 K. The AHI IR10 has no polar counterpart, and its closest polar proxy is IR11. If anything, the AHI IR10 also appears biased several tenths of a Kelvin cold.

Table 2. The nighttime O-M mean biases, standard deviations, and number of clear-sky ocean pixels (NCSOP) for 2 June 2015.

Band Name	Mean, K				SD, K			
	H-8	**S-NPP**	**Aqua**	**Terra**	**H-8**	**S-NPP**	**Aqua**	**Terra**
IR37	−0.51	−0.04	−0.26	0.02	0.39	0.33	0.33	0.32
IR86	−0.82	−0.60	−0.33	1.13	0.42	0.46	0.47	0.49
IR10	−0.79				0.50			
IR11	−0.86	−0.54	−0.51	−0.54	0.60	0.53	0.54	0.52
IR12	−1.09	−0.64	−0.67	−0.70	0.69	0.63	0.62	0.59
	NCSOP (million)				18.6	46.9	18.2	17.8

By and large, all AHI BTs are in-family with their polar counterparts which is, by itself, an encouraging result. Biases range from 0.2–0.3 K in the longwave bands, IR86-IR11. The way how the CRTM coefficients are defined and calculated, can contribute up to several tenths of a Kelvin which may explain, at least a part of these biases [14]. In IR37 and IR12, biases are larger, from 0.4–0.5 K, and are more likely to be caused by the SRF differences or possible uncertainties in the AHI calibration. To independently verify and complement the RTM-based radiance monitoring, hyperspectral sensors such as the Atmospheric Infrared Sounder (AIRS) onboard Aqua, the Infrared Atmospheric Sounding Interferometer (IASI) onboard Metop satellites, and the cross-track infrared sunder (CrIS) onboard S-NPP may be explored (e.g., [19,20]).

The fact that all AHI bands are biased cold may also suggest a larger residual cloud contamination in the ACSPO AHI data compared to the corresponding polar products. Note, however, that the initial implementation of the ACSPO clear-sky mask for AHI was aimed to be conservative. Visual inspection of the AHI SST imagery indeed confirms that the cloud leakages do not exceed those in the polar products (*cf*. e.g., Figure 3), and are unlikely to be the only (or the main) cause of the observed negative AHI biases. Work continues to fine-tune the ACSPO clear-sky mask and re-evaluate the AHI O-M biases.

Figure 5 shows the O-M biases in IR10 and IR11 on 2 June 2015 as a function of the LT (*cf*. Figure 2). (Note that the diurnal cycle in the O-M is mostly attributed to the "O" term because the "M" term is produced from the daily first-guess "foundation" CMC L4 (which most closely represents the diurnal minimum, typically achieved at night before the sunrise), whereas the six-hourly GFS profiles have only secondary effect in the window bands. The polar curves were obtained by a parallel shift of the AHI IR11 curve and anchoring it to the most populated nighttime polar bin. (Note that this fit may not go through all remaining polar bins, including daytime, due to noise in the data which is expected to increase in the less populated data bins.) The diurnal cycle goes through the minimum at ~4–5 a.m., then warms up reaching its peak at 1–2 p.m., and gradually cools off again. The amplitude of the diurnal cycle in the IR11 is ~0.42 K. For comparison, the diurnal cycle in GOES BTs in a comparable IR11 band was estimated to be ~0.55 K [21].

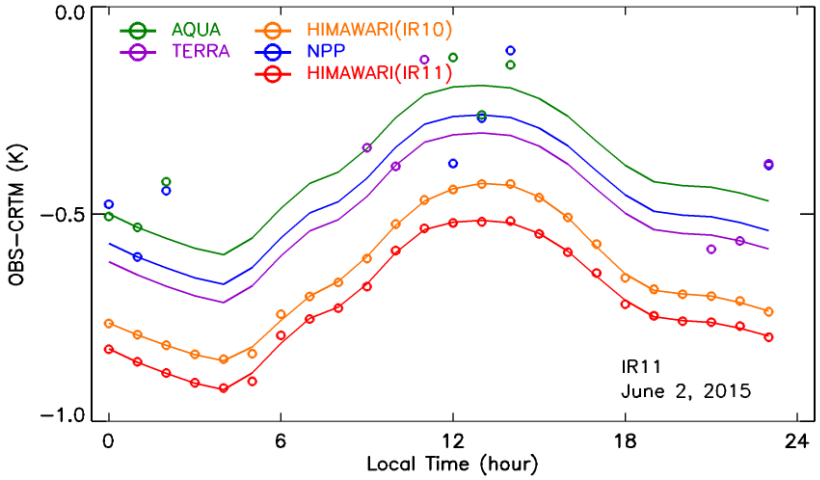

Figure 5. Mean O-M biases over the H8 domain as a function of LT on 2 June 2015 for S-NPP VIIRS, Terra and Aqua MODIS (IR11) and AHI (IR10 and IR11). The polar curves are obtained by a parallel shift of the AHI IR11 curve, and anchoring to the respective most populated nighttime polar bins.

3.2. Stability of the O-M Biases and Double Differences (DDs)

In this section, one month of data from 28 May to 27 June 2015 is analyzed to verify the stability and representativeness of the one day analyses in the previous section.

Figure 6 shows the time-series of the hourly O-M biases in the five SST bands. It is produced as Figure 5 but for a one month time period. Two observations are worth noting. First, the diurnal cycle is much larger in IR37 than in all other bands. This is due to the effect of solar reflectance in this band during the daytime, which is not modeled fully accurately in the current CRTM [22]. The other observation is that the O-M biases are relatively stable in time and do not show obvious systematic changes. However, The day-to-day changes in the geo and polar O-M data (by several tenths of a Kelvin) appear to occur "in-phase", likely due to the unstable "M" term (*i.e.*, unstable CMC SST and the GFS atmospheric profiles first guess fields used as input into CRTM), which will cancel out when the corresponding DDs are calculated.

The nighttime DDs are plotted in Figure 7. For each day, only one data point out of 24 h is plotted, representing the most populated nighttime polar bin. Although the LTs are consistent within each bin, the BTs may nevertheless slightly differ, because the corresponding samples are not spatially collocated point-by-point (as it is done, for instance, in the simultaneous nadir overpasses analyses [23]). Using the most populated nighttime bin does minimize the effect of the diurnal cycle on cross-platform comparisons. Also, using the most statistically significant sample (bin) helps to suppress the residual random noise in the data. All observations made earlier for only one day of data, 2 June 2015 (summarized in Table 2 and discussed in previous section), continue to hold, including in particular the relative signs and magnitudes of the cross platform biases. However, Figure 7 now additionally confirms that the statistics in Table 2 are representative and stable in time.

The AHI IR37 is biased ~−0.47 K cold relative to the S-NPP VIIRS. Terra and Aqua disagree by ~0.25 K, with Terra being closer to the VIIRS. This observation was already made earlier [14] and is now additionally confirmed. In the newly analyzed IR86, AHI BTs are biased cold by ~−0.23 K, whereas both Aqua and Terra are biased warm, by +0.24 K and +1.72 K, respectively. The large Terra bias has been documented elsewhere [18] and is independently confirmed here. In the two longwave bands, AHI BTs are again biased low, from ~−0.3 K in IR11 to ~−0.4 K in IR12.

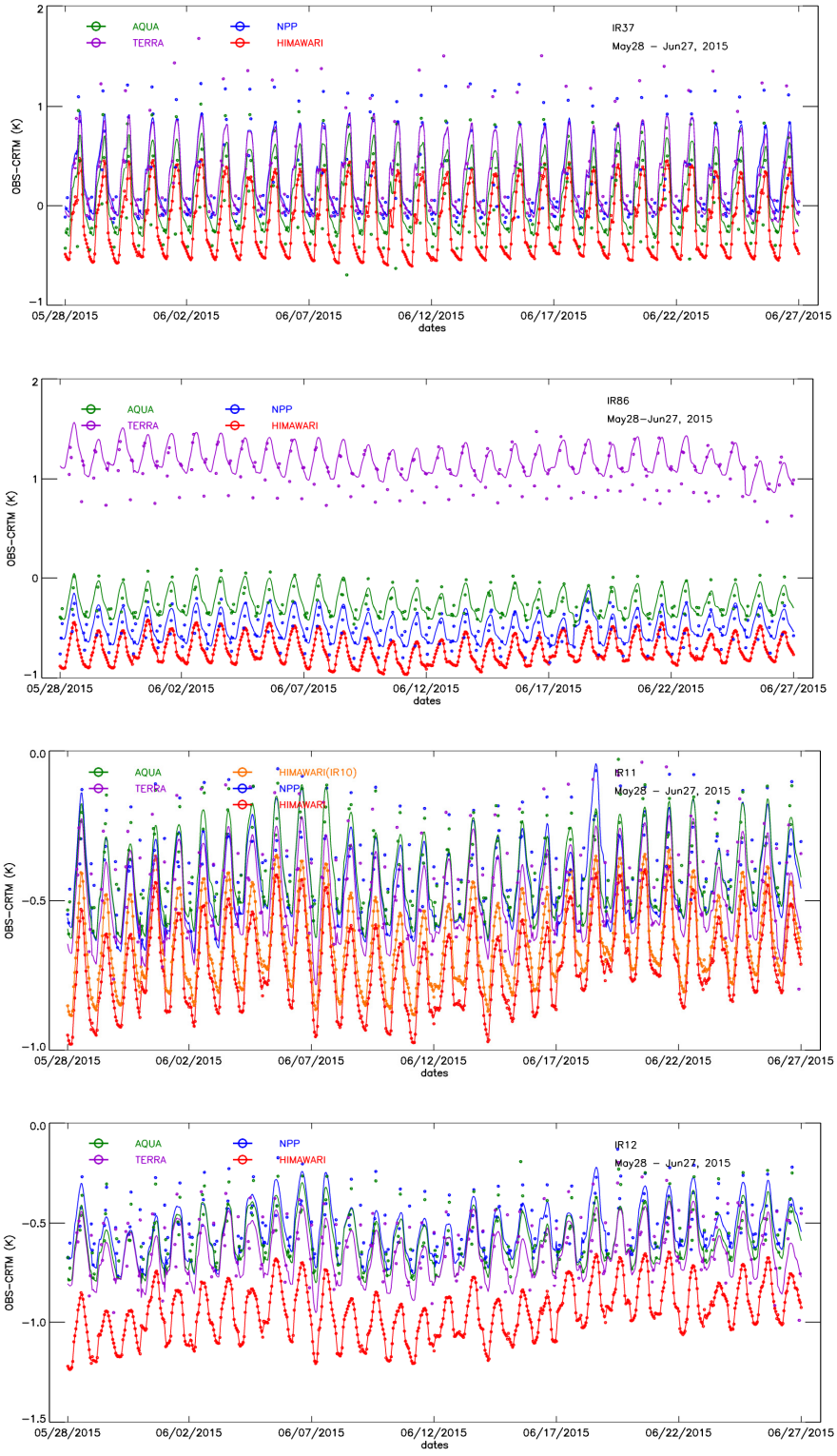

Figure 6. Time-series of the O-M biases for AHI, VIIRS, and MODISs for all five SST bands. The diurnal curves for the VIIRS and MODIS are generated using the same method as in Figure 5.

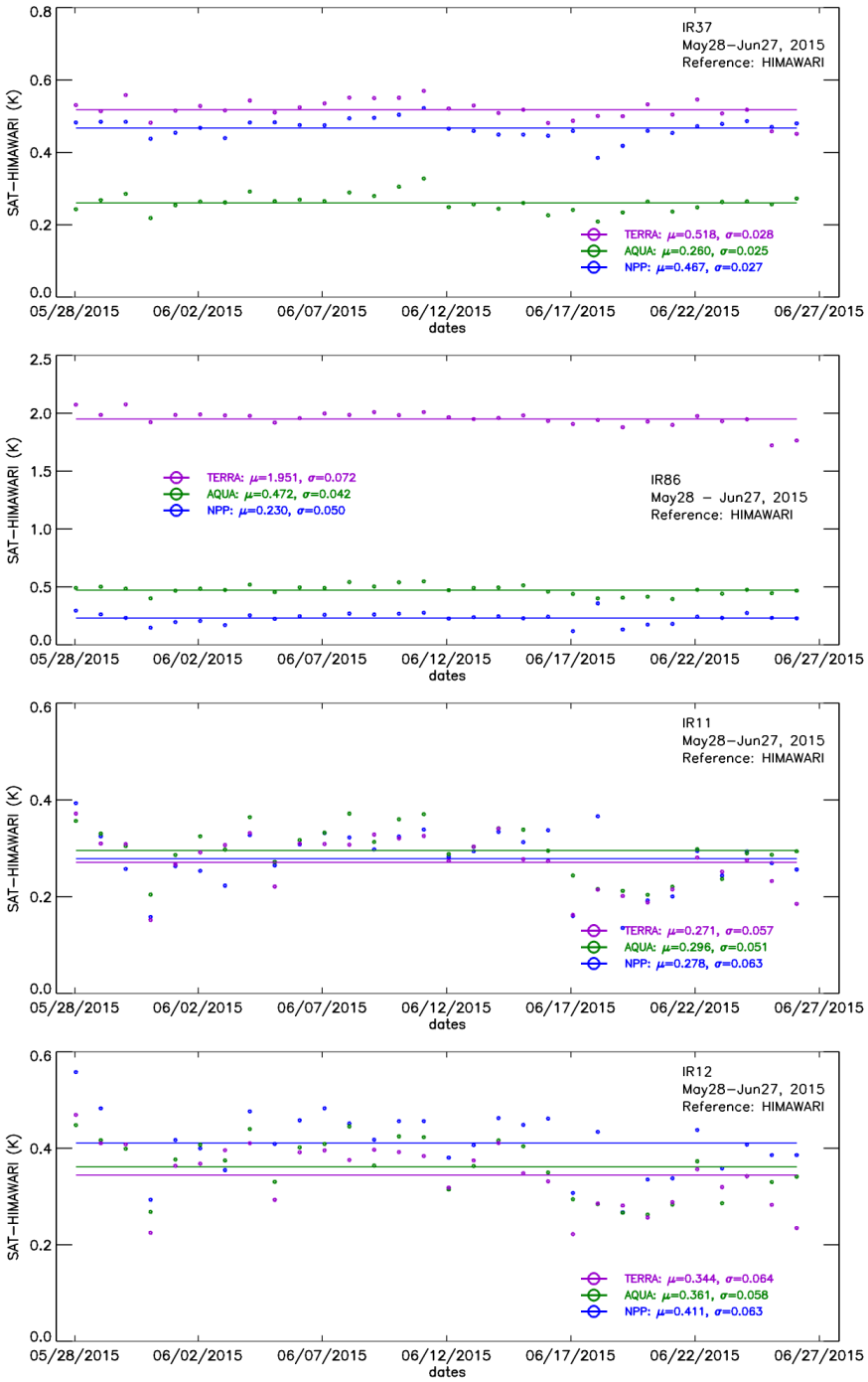

Figure 7. Double differences (DDs) calculated from Figure 6 using Equation (1). For each day, only one data point (out of 24 in Figure 6) is saved corresponding to the most populated polar nighttime bin (which is always 1:30 a.m. for the S-NPP and Aqua and 10:30 p.m. for the Terra—*cf.* Figure 2). Horizontal lines represent mean values over the 30 days. Corresponding mean and standard deviation statistics are also superimposed.

4. Conclusions and Future Work

NOAA is generating an experimental ACSPO SST product from the newly-launched AHI onboard Himawari-8. To support this product, O-M biases in five AHI IR SST window bands at IR37, IR86, IR10, IR11, and IR12 have been calculated and compared against the better understood and characterized VIIRS and MODIS. The objectives are to understand the accuracy and stability of the AHI BTs and

check them for consistency with polar SST sensors and, thus, enhance readiness for the launch of the next-generation US geostationary satellite, GOES-R in 2016, which will carry the ABI sensor similar to the AHI. These analyses are critically important to ensure accuracy, stability, and consistency of the different NOAA geostationary and polar SST products. For the first time, two additional SST bands, IR86 and IR10, were analyzed, to facilitate their use in the ACSPO clear-sky mask and improved SST algorithms.

The major conclusion from our analyses is that all AHI bands are largely in-family with their polar counterparts, but biased cold by -0.25 to -0.5 K, depending upon the band. Additionally, Terra IR86 is biased high by 1.5 K due to electronic crosstalk. The diurnal variability (DV) of the O-M biases for AHI was applied to polar data by anchoring the AHI DV curves to the most populated corresponding nighttime polar bin. The DV in IR37 is much larger than in the other IR bands, due to the effect of solar reflectance in this band during the daytime which is modeled not fully accurately by the current CRTM. One month time series of O-M biases and double differences indicate that the AHI data are relatively stable and the temporal day-to-day variations are due to the unstable "M" term (*i.e.*, the CMC SST and GFS profiles used as input into CRTM).

Overall, AHI BTs are generally stable in time. Although the negative O-M biases may be, in principle, due to the residual cloud in ACSPO, the initial clear-sky mask in ACSPO AHI product was set conservatively and our experience suggests that these factors cannot fully explain the observed magnitudes of the biases. The other possible cause is the way the CRTM coefficients are calculated. The accuracy of the CRTM simulations in MICROS may be independently verified using the hyperspectral infrared sensors, such as the AIRS, IASI, and CrIS as references, similarly to the current JMA implementation [24]. Work is underway to attribute, minimize, and reconcile the O-M biases, and improve their utility for the evaluation of sensor performance for both geo and polar data. However, our experience suggests that these factors are unlikely to fully explain all of these cold biases and, at least a part of them, may be due to the uncertainties in AHI calibration and characterization.

The future work will be adding AHI SST bands in MICROS, including two new bands, IR86 and IR10. The work with the AHI sensor calibration team will continue towards understanding of the root cause of the cold AHI sensor BT biases, and their minimization. The ABI will be added in MICROS when the GOES-R is launched, and compared with the geo AHI and polar VIIRS and MODIS sensors.

Acknowledgments: This work is supported by the JPSS and GOES-R Program Offices, and by the NOAA Product System Development and Implementation (PSDI) and Ocean Remote Sensing Programs. Xingming Liang acknowledges the CSU CIRA research scientist fellowship. Thanks go to Boris Petrenko, Irina Gladkova for their Himawari-8 ACSPO analyses and productive discussions. Yury Kihai, John Stroup, Yaoxian Huang, and John Sapper of NOAA also contributed to the ACSPO development, data collection and analyses, and provided critical feedback and advice. Thanks also go to Fred Wu, co-lead of the NOAA geo calibration team, and to the JAXA and JMA for providing timely and highly accurate AHI L1b data. Thanks to Yong Chen of the NOAA Joint Center for Satellite Data Assimilation (JCSDA) for providing the spectral radiance data plotted in Figure 1. Thanks to Xiaoxiong Xiong of NASA, Junqiang Sun and Changyong Cao of NOAA STAR for helpful discussions and to Quanhua Liu, Paul Van Delst, David Groff and Fuzhong Weng of the JCSDA for providing the CRTM. We also thank three anonymous reviewers for constructive suggestions. The views, opinions, and findings contained in this report are those of the authors and should not be construed as an official NOAA or U.S. Government position, policy, or decision.

Author Contributions: Xingming Liang performed analyses of the data, drafted an initial version of the manuscript, and worked with co-authors on its improvements. Alexander Ignatov significantly contributed to discussions, data analyzes and manuscript preparation. Maxim Kramar set up the ACSPO system to process AHI L1b data, optimized its performance, worked with the calibration team to improve and better handle the AHI data, and produced a high quality Himawari-8 L2 SST product. Fangfang Yu helped with spectral response functions for different sensors and discussions.

Conflicts of Interest: The authors declare no conflict of interest.

References

1. Cao, C.; Xiong, X.; Blonski, S.; Liu, Q.; Uprety, S.; Shao, X.; Bai, Y.; Weng, F. Suomi NPP VIIRS sensor data record verification, validation, and long-term performance monitoring. *J. Geophys. Res.* **2013**, *118*, 11664–11678. [CrossRef]
2. Cao, C.; DeLuccia, F.J.; Xiong, X.; Wolfe, R.; Weng, F. Early on-orbit performance of the Visible Infrared Imaging Radiometer Suite (VIIRS) onboard the Suomi National Polar-orbiting Partnership (S-NPP) Satellite. *IEEE Trans. Geosci. Remote Sens.* **2014**, *52*, 1142–1156. [CrossRef]
3. Xiong, X.; Butler, J.; Chiang, K.; Efremova, B.; Fulbright, J.; Lei, N.; Mclntire, J.; Oudrari, H.; Sun, J.; Wang, Z.; *et al*. VIIRS on-orbit calibration methodology and performance. *J. Geophys. Res.* **2014**, *119*, 5065–5078. [CrossRef]
4. Schmit, T.J.; Gunshor, M.M.; Menzel, W.P.; Gurka, J.J.; Li, J.; Bachmeier, S. Introducing the next-generation advanced baseline imager on GOES-R. *Bull. Am. Meteor. Soc.* **2005**, *86*, 1079–1096. [CrossRef]
5. Murata, H.; Takahashi, M.; Kosaka, Y. VIS and IR Bands of Himawari-8/AHI Compatible with Those of MTSAT-2/Imager. Available online: http://www.data.jma.go.jp/mscweb/technotes/msctechrep60.pdf (accessed on 16 December 2015).
6. Okuyama, A.; Andou, A.; Date, K.; Hoasaka, K.; Mori, N.; Murata, H.; Tabata, T.; Takahashi, M.; Yoshino, R.; Bessho, K. Preliminary validation of Himawari-8/AHI navigation and calibration. *Proc. SPIE 9607* **2015**. [CrossRef]
7. Japan Meteorological Agency Himawari-8 Advanced Himawari Imaer (JMA AHI) Webpage. Available online: http://www.data.jma.go.jp/mscweb/en/himawari89/himawari89plan.html (accessed on 16 December 2015).
8. Liang, X.; Ignatov, A.; Kihai, Y. Implementation of the Community Radiative Transfer Model (CRTM) in Advanced Clear-Sky Processor for Oceans (ACSPO) and validation against nighttime AVHRR radiances. *J. Geophys. Res.* **2009**, *114*. [CrossRef]
9. Petrenko, B.; Ignatov, A.; Kihai, Y.; Heidinger, A. Clear-sky mask for the advanced clear-sky processor for oceans. *J. Atmos. Oceanic Technol.* **2010**, *27*, 1609–1623. [CrossRef]
10. Han, Y.; van Delst, P.; Liu, Q.; Weng, F.; Yan, B.; Treadon, R.; Derber, J. *Community Radiative Transfer Model (CRTM)—Version 1*; NOAA Technicl Report NESDIS 122. NOAA: Silver Spring, MD, USA, 2006.
11. National Centers for Environmental Prediction Global Forecast System (NCEP GFS) webpage. Available online: http://www.emc.ncep.noaa.gov/index.php?branch=GFS (accessed on 6 November 2015).
12. Brasnett, B. The impact of satellite retrievals in a global sea-surface-temperature analysis. *Q. J. R. Meteorol. Soc.* **2008**, *134*. [CrossRef]
13. Liang, X.; Ignatov, A. Monitoring of IR clear-sky radiances over oceans for SST (MICROS). *J. Atmos. Oceanic Technol.* **2011**, *28*. [CrossRef]
14. Liang, X.; Ignatov, A. AVHRR, MODIS, and VIIRS radiometric stability and consistency in SST bands. *J. Geophys. Res.* **2013**, *118*. [CrossRef]
15. Monitoring of IR Clear-Sky Radiances over Oceans for SST (MICROS) Webpage. Availabe online: http://www.star.nesdis.noaa.gov/sod/sst/micros (accessed on 24 February 2016).
16. Griffin, M.K.; Burke, H.K.; Kerekes, J.P. Understanding radiative transfer in the midwave infrared, a precursor to full spectrum atmospheric compensation. *Proc. SPIE 5425* **2004**. [CrossRef]
17. Kilpatrick, K.A.; Podestá, G.; Walsh, S.; Williams, E.; Halliwell, V.; Szczodrak, M.; Brown, O.B.; Minnett, P.J.; Evans, R. A decade of sea surface temperature from MODIS. *Remote Sens. Environ.* **2015**, *165*, 27–41. [CrossRef]
18. Sun, J.; Madhavan, S.; Xiong, X.; Wang, M. Long-term drift induced by the electronic crosstalk in Terra MODIS Band 29. *J. Geophys. Res.* **2015**, *120*. [CrossRef]
19. Wang, L.; Han, Y.; Jin, X.; Chen, Y.; Tremblay, D. Radiometric consistency assessment of hyperspectral infrared sounders. *Atmos. Meas. Tech.* **2015**, *8*. [CrossRef]
20. Wang, L.; Cao, C. On-orbit calibration assessment of AVHRR longwave channels on Metop-A using IASI. *IEEE Trans. Geosci. Remote Sens.* **2008**, *46*, 4005–4013. [CrossRef]
21. Garand, L. Toward an integrated land–ocean surface skin temperature analysis from the variational assimilation of infrared radiances. *J. Appl. Meteor.* **2003**, *42*, 570–583. [CrossRef]

22. Liang, X.; Ignatov, A.; Han, Y.; Zhang, H. Validation and Improvements of Daytime CRTM Performance Using AVHRR IR 3.7 um Band. Available online: https://ams.confex.com/ams/pdfpapers/170593.pdf (accessed on 24 February 2016).
23. Cao, C.; Weinreb, M.; Xu, H. Predicting simultaneous nadir overpasses among polar-orbiting meteorological satellites for the inter-satellite calibration of radiometers. *J. Atmos. Ocean. Technol.* **2004**, *21*, 537–542. [CrossRef]
24. JMA Himawari-8 AHI IR Inter-calibration with AIRS, IASI-A/B and CrIS webpage. Available online: http://www.data.jma.go.jp/mscweb/data/monitoring/gsics/ir/monit_geoleoir.html (accessed on 18 January 2016).